11-01990

LA-UR-

Approved for public release; distribution is unlimited.

Title: Performance of the Los Alamos National Laboratory spallation-neutron driven solid deuterium ultra-cold neutron source

Author(s): A. Saunders M. Makela, H. O. Back J. Boisavain, L. J. Broussard T. J. Bowles, R. Carr S. A. Currie, B. Filippone, A. García Peter Geltenbort K. P. Hickerson , R. Hill, J. Hoagland, A. T. Holley, G. Hogan, T. M. Ito, Steve Lamoreaux, J. Liu, R.R. Mammei J. Martin D. Melconian M. P. Mendenhall, C. L. Morris, R. N. Mortensen, R. W. Pattie Jr. , M. Pitt, B. Plaster J. Ramsey, R. Rios S. J. Seestrom, E.

Intended for: Review of Scientific Instruments

Los Alamos
NATIONAL LABORATORY
EST. 1943

Los Alamos National Laboratory, an affirmative action/equal opportunity employer, is operated by the Los Alamos National Security, LLC for the National Nuclear Security Administration of the U.S. Department of Energy under contract DE-AC52-06NA25396. By acceptance of this article, the publisher recognizes that the U.S. Government retains a nonexclusive, royalty-free license to publish or reproduce the published form of this contribution, or to allow others to do so, for U.S. Government purposes. Los Alamos National Laboratory requests that the publisher identify this article as work performed under the auspices of the U.S. Department of Energy. Los Alamos National Laboratory strongly supports academic freedom and a researcher's right to publish; as an institution, however, the Laboratory does not endorse the viewpoint of a publication or guarantee its technical correctness.

Form 836 (7/06)

To be submitted to: Review of Scientific Instruments

Performance of the Los Alamos National Laboratory spallation-neutron driven solid deuterium ultra-cold neutron source

A. Saunders[1], M. Makela[1], H. O. Back[2], Y. Bagdasarova, J. Boissevain[1], L. J. Broussard[3], T. J. Bowles[1], R. Carr[4], S. A. Currie[1], B. Filippone[4], A. García[5], Peter Geltenbort,[6] K. P. Hickerson [4], R. Hill[1], J. Hoagland[2], S. Hoedl[5], A. T. Holley[2], G. Hogan[1], T. M. Ito[1,4], Steve Lamoreaux[1,7], J. Liu[4,8], R.R. Mammei[9], J. Martin[4,10], D. Melconian[11], M. P. Mendenhall[4], C. L. Morris[1], R. N. Mortensen[1], R. W. Pattie Jr. [2], M. Pitt[9], B. Plaster[12], J. Ramsey[1], R. Rios[13], Anne Sallaska[5], S. J. Seestrom[1], E. I. Sharapov[14], S. Sjue[5], W. E. Sondheim[1], W. Teasdale[1], A. R. Young[2], B. VornDick[2], R. B. Vogelaar[9], and Yanping Xu[2]

Abstract In this paper we describe the performance of the Los Alamos spallation-driven solid-deuterium Ultra Cold Neutron (UCN) source. Measurements of the cold neutron flux, direct measurements of the very low energy neutron production rate, and measurements of the UCN rates at the exit from the biological shield are presented and compared to Monte Carlo predictions. The cold neutron rates compare well with predictions from the Monte Carlo code MCNPX. The source is shown to perform as modeled.

PACS: 29.25.Dz, 28.20.-v, 28.20.Cz, 28.20.Fc, 28.20.Gd

---

1 *Los Alamos National Laboratory*, Los Alamos, NM 87544, USA
2 *Department of Physics, North Carolina State University*, Raleigh, North Carolina 27695, USA
3 *Department of Physics, Duke University*, Durham, North Carolina 27708, USA
4 *Kellogg Radiation Laboratory, California Institute of Technology*, Pasadena, California 91125, USA.
5 Department of Physics, University of Washington, Seattle, Washington 98195, USA
6 Institut Laue-Langevin, 38042 Grenoble Cedex 9, France
7 Yale University, Department of Physics, PO Box 208120, New Haven, Connecticut 06520-8120, USA
8 Department of Physics, Shanghai Jiao Tong University, Shanghai, 200240, China
9 Department of Physics, Virginia Tech, Blacksburg, Virginia 24061, USA
10 University of Winnipeg, Winnipeg, MB R3B 2E9 Canada.
11 Cyclotron Institute, Texas AM University, College Station, Texas 77843, USA
12 Department of Physics and Astronomy, University of Kentucky, Lexington, Kentucky 40506, USA
13 Department of Physics, Idaho State University, Pocatello, Idaho 83209, USA
14 Joint Institute for Nuclear Research, 141980, Dubna, Russia

To be submitted to: Review of Scientific Instruments

Introduction

Ultra cold neutrons are defined as neutrons that can be trapped in material bottles and guides because their energies are less than the Fermi potential,

$$V_F = \frac{2\pi\hbar^2}{m} Na \quad .$$

^{58}Ni exhibits one of the largest potentials of available materials, 342 nV. Neutrons with energies below this (or velocities below 8.09 m/s) can be trapped in a ^{58}Ni bottle. Two reviews highlight the wide variety of physics that can be performed using trapped UCN.[1, 2]

In the past decade experiments have demonstrated several advantages of using ultra-cold neutrons for beta decay experiments. Measuring the decay of neutrons bottled in material bottles eliminates systematic errors associated with defining the volume that plague lifetime experiments with cold neutron beams[3-6] and therefore allows more precise measurements.[7-12] More recently, results obtained with the LANSCE UCN source[13, 14] have demonstrated that the high polarizations and low backgrounds that can be obtained with spallation driven, pulsed UCN sources can reduce the systematic errors in measuring the spin dependence of neutron beta decay.[15, 16]

Pokotilovski pointed out the advantages of UCN production in SD_2 at pulsed neutron sources[17] and the use of spallation as a pulsed source was suggested by the Gatchina group.[18-20] New UCN sources, using superthermal production[1] with either superfluid Helium or solid deuterium, are being built at several facilities.[21-24]

The lifetimes of UCN, measured in solid para-deuterium, [25] are long enough to obtain high densities in a spallation drive source, in agreement with theoretical calculations,[26] and high densities were measured in a prototype source.[27] UCN production rates measured in experiments at PSI[28] and at LANSCE[29] have verified the earlier work in more quantitative experiments.

Here we report on results that have been obtained with a spallation driven pulsed UCN source, driven with protons provided by the 800 MeV Los Alamos Neutron Science Center (LANSCE) linear accelerator at the Los Alamos National Laboratory. The source moderates and converts spallation neutrons, produced in a tungsten target, to UCN in a windowless solid deuterium volume inside of a UCN guide system. The neutrons are transported through a stainless steel guide system to an experimental area where they can be used for experiments. In this paper we describe the design of the source, measurements and predictions of the cold and UCN production rates. We compare Monte Carlo predictions of the UCN transport times and flux through the guide system, and use the Monte Carlo predictions to predict the densities available for experiments.

Design

The details of the source are shown in the schematic drawing in **Error! Reference source not found.**. Protons from the LANSCE 800 MeV accelerator are delivered to a 12 cm long helium gas-cooled tungsten alloy-spallation target. Recently the target shape has been changed to increase the amount of tungsten to be closer to the optimum amount. This has

increased the UCN rates by ~ 50%. The target is surrounded by a room temperature beryllium reflector, in which a liquid helium cooled volume of solid deuterium (SD_2) is embedded. The SD_2 volume, 20 cm diameter and 5.7 cm high, is contained in an aluminum cryostat that is coated with ^{58}Ni to reflect and contain the UCN. This entire assembly is surrounded by approximately 1 m of reactor grade graphite. The solid deuterium volume is surrounded by a 1 cm thick layer of polyethylene beads with an effective density of 0.5-0.6 g/ cm^3, cooled by some of the boil off gas from the SD_2. The temperature of the polyethylene depends on the proton current delivered to the W-target and was around 150K at an average current of 5.8 μA. Measurements indicate only a weak dependence of the UCN production rate on the polyethylene temperature. A significant amount of moderation is provided by the SD_2.

The aim of this design is to locate the solid deuterium volume as close to the spallation target as possible in order to take advantage of the high neutron densities possible in spallation neutron production. Since only ~20 MeV of thermal energy is deposited in the target for each spallation neutron produced, compared to ~200 MeV per neutron in a reactor, the neutron density in a spallation source can be higher for a given cooling capability. However, because of the small source volume this density falls quickly as one moves away from the spallation target. The challenge is to provide enough cooling to the solid deuterium to keep the temperature sufficiently low so as not to impact the UCN life times in the target due to thermal up scatter[1] while the beam is on. The source of heating is both charged particles and gamma rays produced in beam target interactions. The lower part of the target was constructed from an aluminum alloy in order to keep the heat load from the target walls to a minimum. Thermal isolation between the solid deuterium volume and the upper target region was provided by an explosively bonded aluminum to stainless steel thermal break. The temperature of the guide above the thermal break could be controlled by flowing boil off helium from the SD_2 volume through a heat exchanger attached to the outer target wall.

The inside wall of the cryostat volume and vertical guide was sputter coated with 200 nm of ^{58}Ni. The Fermi potential of the SD_2 (102 nV)boosts the neutrons energy when passing from the SD_2 into vacuum; gravity was used to cancel this effect with a 1 m vertical section of 18 cm diameter guide before the horizontal guide section out of the shield wall. The 342 nV potential ensured that all of the neutrons that could be transported by stainless steel (189 nV potential) into the experimental area were trapped in the lower volume of the source.

A butterfly (flapper) valve was attached to the bottom of the vertical guide. This was actuated by a rotation shaft that exited from the top of the system and was driven by a stepping motor. The minimum opening and closing time of the flapper value was about 0.1 sec.

The beam from the accelerator was typically 10-mA of protons, delivered in 5 pulses each 600 μsec long delivered at a rate of 20 Hz, with a gap between groups of pulses of 5.0 seconds. The total charge delivered per pulse group is 30 μC in 0.2 s or a current of 150 μA when the UCN valve is open. The average current delivered to the target in this mode is 5.8 μA.

Previous design calculations[13, 30] predicted that the total cold neutron (CN) flux, Φ_{CN}, through the solid deuterium volume would be about 3 CN/proton delivered to the tungsten target (this gives cold neutron flux density of 6×10^{10} /cm^2/μA). The UCN production was predicted to be 250 UCN/cm^3 /μC inside the SD_2 volume. Because the source performance fell below these expectations we have conducted measurements of the flux from the new UCN source and performed calculations with the latest MCNP5/MCNPX codes and their standard data libraries.[31] These are described below.

Cold Neutron performance

Measurements of the cold neutron flux in the target volume were accomplished using two methods: 1) argon activation and 2) direct counting cold neutrons with the ^{3}He detector of known efficiency in a time of flight (TOF) experiment.

a) Activated Argon Cold Neutron Flux Measurement

An argon activation experiment was performed by freezing 15.2 g of argon in the target volume, delivering a small amount of proton charge through the tungsten target, and then recovering some of the gas and counting gamma rays produced by the beta decay of ^{41}Ar. The argon was preloaded into a known volume of 7.9 l at 1.3×10^5 Pa (Figure 2). This was subsequently opened to the source and the temperature was allowed to equilibrate. The final pressure was 6.3×10^3 Pa. The source volume is calculated to be 159 l.

The source was then cooled to 60 K (freezing the argon into the cold volume of the source) and exposed to the neutron flux produced by 1.52×10^{15} protons irradiating the tungsten spallation target. The polyethylene (cold moderator) temperature for this irradiation was 155 K. After the irradiation, the source was warmed until the pressure in the loading volume was 4.9×10^3 Pa (82% recovery). The loading volume was closed off from the rest of the system, the remaining argon in the source was pumped out, and the 1.2 MeV gamma rays from the beta decay of ^{41}Ar ($t_{1/2}$ 126 sec) in the loading volume were counted. A spectrum is shown in Figure 3.

The product of photopeak efficiency and solid angle for the High Purity Germanium (HPGe) detector was measured by mounting a ^{60}Co source of known activity at the gas volume location and comparing rates of the 1.17 and 1.33 MeV peaks to the known decay rate. From these measurements, the ^{41}Ar production rate per proton was calculated to be 6.5×10^{-4} integrated over the neutron spectrum. This compares to the MCNP prediction of 7.1×10^{-4}. Using the thermal neutron capture cross section of ^{40}Ar of 0.66 b, a *1/v* energy dependence, and assuming a Maxwellian density at the neutron temperature of 155 K allows the cold neutron flux in the source to be calculated from these measurements, if the relative contribution from cold neutrons to the total activation is known. For the latter quantity we took the value of 60% calculated by the MCNP code. This gives a neutron flux of 0.84±0.17 neutrons/proton through the SD_2 source area in the absence of SD_2, which gives a flux density of $1.7\pm0.3\times10^{10}$/cm^2/μA. The peak neutron flux is about 1.33×10^{13}/cm^2, about 1/10 of that available in the core of the ILL reactor. More importantly, the thermal loads allow operation of our source at 5k. A 20% uncertainty has been assigned to account for our lack of knowledge of the exact geometry of the frozen argon.

a) Time of flight Cold Neutron Flux Measurement

The TOF experiment to benchmark the MCNP cold neutron flux was performed with a ^{3}He detector mounted on the top of the 2-m long iron shielding plug. The plug had two vertical channels of 2-cm diameter, one with a 0.75 mm of aluminum window and the other with a 2 mm of pyrex window. The detector viewed the cold neutron source through both channels. The neutron flight path in this geometry was 3.60 m. The efficiency of the detector for 25-meV neutrons was 0.19. A pulse-height spectrum is shown in Figure 3. For these measurements protons were delivered to the target in 250 ns long pulses of $\sim 1.4 \times 10^{10}$ protons at a rate of one pulse per second. The proton fluence was measured with a Bergoz coil to a precision of several percent. The arrival time of pulses from the neutron detector (TOF) was measured as a function of time after the proton pulse. A typical TOF spectrum with the polyethylene at a temperature of 220K, measured with the source empty (no solid deuterium) is shown in Figure 6. The time of the proton pulse is at t=0 (the width of channels is 10 microsecond). The time of 2000 μs corresponds to the neutron energy of 40 meV, while the channel 4000 μs corresponds to 6 meV. The total number of protons through the tungsten target in this run was 5.2×10^{13}.

Figure 6 also shows the time of-flight spectrum measured with the UCN solid deuterium source SD_2 built from the deuterium gas in the cryostat with the polyethylene temperature of 60K. The spectrum demonstrates a considerable enhancement of the relative contribution of neutrons below the 6-meV energy. The total number of protons through the tungsten target in this run was 5.7×10^{13}.

Deducing the shape of the cold neutron energy spectrum from these data requires a complicated deconvolution of the TOF-spectrum due to the energy dependent moderation time in the source (400-600 microsecond) which dominates the resolution function. This width is comparable to the width of the measured spectrum. The integral over the spectrum, however, does not depend on the resolution function; therefore it can be directly compared with the MCNP modeling. We performed such a comparison for neutron flux at the detector position after taking account of the energy dependent ^{3}He detector efficiency. For the first spectrum the integral below 100 meV is 1.56×10^5 neutrons per μC of protons, while the corresponding MCNP prediction is 1.70×10^5per μC. For the second spectrum the integrals below 25 meV are 0.75×10^5 per μC of protons and 0.86×10^5 per μC respectively measured and predicted. In both cases the agreement is within 20%.

Here we give a few details of the MCNP simulation, which was performed with the codes MCNP5[32] and MCNPX.[33] We used the $S(\alpha,\beta)$ option of the MCNP cross sections for SD_2, graphite, beryllium and the Maxwellian MCNP gas model cross sections for other materials including polyethylene. Replacing, in the presence of SD_2, the 150K temperature polyethylene by the MCNP 20K temperature solid methane with an equivalent concentration of the hydrogen atoms we had found only 25% increase in the cold neutron flux which gave confidence in the use the MCNP 150K polyethylene data and not the 70K polyethylene scattering kernel, which is absent in the MCNP5 data library.

We used the geometry for the LANL ultra cold neutron source, which takes into account all essential features of the setup shown in Figure 1, developed by Yanping Xu.[34] The small solid angle of the collimation prevented a direct simulation of the ^{3}He detector counts in the

original geometry because of the very low transmission. Therefore, the flux modeling at the ^{3}He detector was performed in two stages. First, the neutron flux entering the upper hemisphere from the area of the SD_2 cell seen by the detector was simulated directly with the proton source in the tungsten target. Second, the solid angle from this area through the collimator to the detector was modeled by placing an MCNP "SDEF surface source" with $\cos(\theta)$ angular distribution on this area. By modeling with different area sizes we determined that uncertainty in the knowledge of area has no influence on the final result for the flux at the detector.

UCN Production

The production of UCN in solid deuterium was measured in the experimental setup shown in Figure 7. The source was cooled and filled with solid deuterium. A detector was installed in the UCN source. It was located about 160 cm above the bottom of the source behind a nickel foil. The detector was mounted to a stainless steel plate that was set on the ledge above the tee for the horizontal guide. The detector had two active regions each 2.2 cm thick separated by a nickel foil. The active area of the detector was $7.8\pm0.2 \times 7.8\pm 0.2$ cm^2.

The detector was filled with a gas mixture of 8×10^4 Pa of CF_4 and $(1.00\pm0.01)\times10^3$ Pa of ^{3}He. A schematic of the detector is given in the figure below. The tungsten target was irradiated with proton pulses and the arrival time of pulses from the detector was measured as a function of time after the proton pulse. The detector response was modeled by tallying only neutrons that were absorbed in the gas. The lifetime for absorption was determined by the ^{3}He pressure to be 3.2 ms. The detector geometry is shown in Figure 8

The detector was configured with an internal voltage divider to place the cathode planes at 1/3 of the potential of the anode planes using a string of 100 MΩ resistors. The cathodes were bypassed to ground through 1 nF capacitors. The outer cathodes were constructed from electro-formed nickel grids with 97% open area. The inner cathode was a solid 25 μm thick nickel foil. The anode/cathode spacing was 0.4 mm.

The detectors were operated at an anode voltage of 3400 V to provide sufficient anode gain to ensure good signal-to-noise ratios while driving the 4.5 m of coaxial cable needed to get the signal out of the shielding package. The signals were amplified in a fast (200 MHz) amplifier with a gain of ~20, and then were fed into an Ortec™ timing filter amplifier. An integration time of 50 ns and a differentiation time of 500 ns gave good signal to noise performance.

The detector was separated from the internal volume by a nickel barrier with a potential of 242 nV and a lifetime of 3.2×10^{-4} sec and a thickness of 0.0025 cm. The SD_2 was modeled with a potential of 108 nV and lifetime of 2.0×10^{-2} sec. The internal guide was modeled with a Fermi potential of 335 nV, a nonspecularity of 0.025, and a loss per bounce of 2.8×10^{-4}.

Data were taken with a 650 μs long beam gate, with a countdown of 10, and at a rate of 1/30 Hz. The charge in each beam pulse was about 0.5 μC. A spectrum from the front detector are shown in Figure 9.

In the calculation, neutrons were chosen from a v^2dv distribution up to 200 m/sec. Arrival times at the detector were tallied. The resulting spectrum was normalized to the data, and

the normalization was used to determine the production rate of neutrons with velocities below 8 m/sec. The normalized distribution is shown along with the data in Figure 9. Data were taken with deuterium in the target and with the target empty. These are also shown in Figure 9.

The transport to the detector of neutrons produced with a Maxwellian energy distribution in the solid deuterium was predicted with a Monte Carlo calculation and normalized to the difference between full an empty. The result is shown in Figure 9. The production rate of UCN (Neutrons with kinetic energies below (380-109 nv) in the solid deuterium (neutrons that are trapped by a 58Ni potential after they receive a 109 nV boost on exiting from the solid deuterium) can be obtained by integrating the distribution. The inferred production density is 85±10 UCN/μC/cm^3.

On the other hand, relying on our successfully benchmarked (see the previous section) MCNP5 prediction of cold neutron flux, we have simulated the cold neutron spectrum for the source. It is shown in Figure 10. The temperature of the polyethylene in this case is 150K. A visible structure is produced by the MCNP data file for solid deuterium at 20K. The flux averaged over the SD_2 volume is 2.0×10^{10} /cm^2/s/μC for neutron energies below 25 meV (this is the energy range effective for UCN production[35]). Comparing this prediction with the argon activation result for the empty source we see a good agreement. Convolving this spectrum, with the deuterium molecular number density of 3×10^{22} / cm^3, with the UCN production cross sections on cold neutron energy measured by Atchison[35] we have calculated the UCN production density to be 107±20 UCN/μC/cm^3, in a good agreement with the experimental result of 85±10 UCN/μC/cm^3. With an average proton beam current of 6 μA, a peak current of 120 μA, the source in principle can achieve a peak UCN density of 110000 UCN/cm^3. In fact, since the volume of the SD_2 only fills 1/3 of the volume below the flapper valve the actual peak densities are only 3000 UCN/cm^3.

We note also that in the latest in-beam study at LANSCE[29] the UCN effective production cross section was measured to be 1.27×10^{-7} b per molecule for the UCN energy range of 0-300 neV, in agreement with the cross sections Atchison[28] when these are integrated over the neutron spectrum from LANSCE flight path FP-12 which is characterized by the neutron temperature of 35K.

The current results can be compared with previous measurements of our prototype source of 460±90 UCN/μC/cm^3.[27] The prototype source had a diameter of 8 cm, a solid polyethylene cooled to 4K and a beryllium reflector cooled to 77K. MCNP modeling suggests the smaller volume and different aspect ratio of the prototype gives a factor of two higher density in the same moderator assembly when compared to the present source. The remaining difference of a factor of two is probably due to the combined effects of a different design and performance of the polyethylene moderator, to different absorption of cold neutrons in the construction materials and to the larger tungsten spallation target used in the prototype.

Transport

Measurements of the UCN flux external to the shielding packaged were used to characterize the overall source and guide performance. The drawings in Figure 4 show the configuration

used for these measurements. The flux from the source could be measured using the main detector by opening the gate valve (labeled in the figure). For normal operation the proton beam was delivered in groups of five 600 μsec long pulses delivered at rate of 20 Hz with a spacing between groups of 5 seconds. The total current in these measurements, measured using the Bergoz coil, was limited to about 5.0 μA by the accelerator safety system, which was unable to integrate the current for the entire spacing between pulses.

The neutron flux and the source lifetime were measured by using UCN detectors[36] external to the shield wall. The transport properties of the source were benchmarked using two measurements. In the first the gate valve was closed and proton groups were delivered to the target at a rate of 1 group every 60 seconds. Measurements were made for three states of the flapper: open, closed and flapping. In the flapping state the flapper was open at the beginning of the pulse group and closed at the end. Opening and closing times were ~0.1 sec. The total time opened was ~.5 seconds.

The source is modeled with a Monte Carlo transport code that includes gravitational, magnetic and material potentials. The system was modeled using a series of connected right circular cylinders. Each cylinder is characterized by a wall Fermi potential, a loss per bounce, a non-specularity fraction, an internal potential, spin dependent potential, and a scatter length. Random origins and directions and velocity for neutrons created in the SD_2 volume were chosen using a pseudo-random number generator. The velocities, v, were picked from a v^2dv phase space distribution with a cut off of 8 m/s in vacuum. The neutron trajectories were modeled by calculating intersections of their parabolic trajectory with guide boundaries. At the earliest intersection they are either absorbed, reflected specularly, reflected diffusely (into a $\cos(\theta)$ angular distribution where θ is measured with respect to the normal from the guide), or passed into a connected guide section. The connections between guides can be opened or closed at different times. This model does not include detailed quantum mechanical models of reflection and transmission from potential barriers or of scattering rough surfaces.

Plots of the rate of UCNs measured in the monitor detector for the flapper open run are shown in Figure 11 and the flapper closed run are shown in Figure 12. The arrival time distribution at early times is sensitive to the non-specularity of the guide surfaces. A single parameter has been used for all of the guides in the model and this was adjusted to fit the region between 1 and 10 seconds in the data presented in Figure 11. Monte Carlo predictions as a function of the non-specularity and the loss per bounce are shown in Figure 11 and Figure 12 respectively. The best fit of $3.0(5)\times10^{-2}$ and $3.53(11)\times10^{-4}$ were obtained for the non-specularity and the loss per bounce respectively.

A potential of 100 nV, a neutron lifetime of 30 msec, and a scatter length of 4 cm were used for the solid deuterium. These were calculated knowing the H-D fraction, the density, and the otho-para ratio of the deuterium. These were $2.\times10^{-3}$, 0.2 g/cm^3, and 1.% respectively when the source was in running condition. The H-D fraction was supplied by the manufacturer of the gas, the density was obtained from xxx, and the para fraction was measured using Raman scattering[37] from a gas sample. Conversion from the room temperature value of 1/3 was accomplished by using a catalytic converter[37] which achieved ~4%, and then by irradiating the source with proton beam which lowered the fraction to ~1% after ~1 week of running at 4 μA.

The surface of the ½ " VCR connection to the monitor connector was not well determined. It was modeled as a vertical section 7 cm long of 1 cm diameter guide with a non-specularity of unity. This was checked by comparing the counting rate in the monitor detector with that in a 7.5 cm diameter guide coupled through a super conducting magnet, the pre polarizer magnet (PPM), that normal held a magnetically embedded aluminum foil that decoupled the source vacuum from the experiment vacuum while polarizing the UCN neutron beam. Measurements of the two monitor counting rates along with the Monte Carlo predictions are shown in Figure 13. This ensures that the transport into the monitor detector is understood to the same level as the transport into the main detector.

The efficiency of the UCN detectors includes several terms: losses in the windows (measured to be ~50%) losses due to wall effects (measured to be 20%), thermal upscattering from the CF_4 (calculated to be 20%) and (geometric loss calculated to be 12%). The net detector efficiency is 0.25(5)%.

This model of the source was applied to data taken during the 2009 and 2010 UCNA running periods. Between these two years the tungsten spallation was changed from a cylinder to a "D" shape that had about twice the mass and was expected to produce more neutrons. The number of neutrons produce in the SD_2 per μC of incident proton fluence was adjusted to reproduce the monitor counting rate with the gate valve closed. This gave 60(12) UCN/μC/cm^3 for the 2009 target and 100(20) UCN/μC/cm^3 for the 2010 target. The normalization for the old target compares well with the number measured with the internal detector of 85±10 UCN/μC/cm^3 and also agrees with the cold neutron density measurements when they are integrated over the UCN production cross sections.

The UCN density achieved external to the shielding wall with the gate valve closed in the UCN guide is 48(10) UCN/cm^3 and 79(16) in 2009 and 2010 running respectively. The model was used to transport UCN though the polarizing system and into the superconducting spectrometer (SCS) that used for UCNA. Significant loss in the density occur in this transport because of the polarization; losses in the high magnetic field regions of the two polarizing guides; losses in loading the SCS where the lifetime is comparable to the loading time loading time; and losses because of the magnetic field boost in the SCS. Figure 14 shows how the density evolves through the transport system. The predicted density achieved in the SCS, obtained by normalizing the calculation to the monitor detector, was 2.0(4) UCN/cm^3 and the predicted beta decay rate was 60(12) which agrees well with the measured decay rate of 40-60, with a peak of 60. This provides an absolute check on the predicted densities inferred from the Monte Carlo calculations and the agreement is good.

Conclusions

The Los Alamos spallation driven UCN source has been commissioned. We have described a set of measurements and simulations that together give confidence that the source is performing as expected. Good agreement has been obtained between performed measurements and predictions based on the MCNP5/MCNPX simulations.

We conclude that with the average proton beam current of 5 μA the UCN densities available for experiments of >80 UCN/cm^3 are competitive with densities which can be provided by sources at research reactors. The polarized density provided for the UCNA experiment of >2

357UCN/cm^3 has allowed this experiment to compete with cold beam measurements of the
358neutron correlation parameter A.

359

360**References**

3611. R. Golub, D. Richardson and S. K. Lamoreaux, *Ultra-cold neutrons.* (New York, NY
362 (United States) ;American Institute of Physics, United States, 1991).
3632. V. K. Ignatovich, *The physics of ultracold neutrons.* (Clarendon Press ; Oxford
364 University Press, Oxford, 1990).
3653. J. Byrne, J. Morse, K. F. Smith, F. Shaikh, et al., Physics Letters B **92B** (3-4), 274-278
366 (1980).
3674. M. Dewey, K. Coakley, D. Gilliam, G. Greene, et al., Nuclear Instruments & Methods in
368 Physics Research, Section A (Accelerators, Spectrometers, Detectors and Associated
369 Equipment) **611** (2-3), 189-192 (2009).
3705. M. S. Dewey, D. M. Gilliam, J. S. Nico, F. E. Wietfeldt, et al., Phys. Rev. Lett. **91** (15),
371 152302/152301-152304 (2003).
3726. J. Last, M. Arnold, J. Doehner, D. Dubbers, et al., Phys. Rev. Lett. **60** (11), 995-998
373 (1988).
3747. W. Mampe, P. Ageron, C. Bates, J. M. Pendlebury, et al., Phys. Rev. Lett. **63** (6), 593-
375 596 (1989).
3768. A. Pichlmaier, J. Butterworth, P. Geltenbort, H. Nagel, et al., Nuclear Instruments &
377 Methods in Physics Research Section A **440** (3), 517-521 (2000).
3789. A. Pichlmaier, V. Varlamov, K. Schreckenbach and P. Geltenbort, Physics Letters B
379 **693** (3), 221-226 (2010).
38010. A. P. Serebrov, PHYSICS-USPEKHI **48** (9), 867-885 (2005).
38111. A. P. Serebrov and A. K. Fomin, Physical Review C **82** (3), 035501 (2010).
38212. B. Yerozolimsky, A. Steyerl, O. Kwon, V. Luschikov, et al., presented at the Neutron
383 Spectroscopy, Nuclear Structure, Related Topics. XII International Seminar on
384 Interaction of Neutrons with Nuclei, Dubna, Russia, 2005 (unpublished).
38513. R. E. Hill, J. M. Anaya, T. J. Bowles, G. L. Greene, et al., presented at the International
386 Workshop on Particle Physics with Slow Neutrons Inst. Laue Langevin, Grenoble,
387 France, 2000 (unpublished).
38814. K. Kirch, T. J. Bowles, B. Fillipone, P. Geltenbort, et al., presented at the Application of
389 Accelerators in Research and Industry. Sixteenth International Conference Denton,
390 TX, USA, 2000 (unpublished).
39115. J. Liu, M. P. Mendenhall, A. T. Holley, H. O. Back, et al., Phys. Rev. Lett.**105** (18),
392 181803 (181805 pp.) (2010).
39316. R. W. Pattie, Jr., H. O. Back, A. R. Young, D. N. C. Triangle Universities Nuclear
394 Laboratory, et al., Phys. Rev. Lett.**102** (1), 012301-012301.012304 (2009).
39517. Y. N. Pokotilovski, Nuclear Instruments & Methods in Physics Research A **356** (2-3),
396 412-414 (1995).
39718. A. Serebrov, V. Mityukhlyaev, A. Zakharov, M. Sazhin, et al., presented at the Fifth
398 Cryogenics '98 IIR International Conference, Proceedings, 177 blvd Malesherbes, F-
399 75017 Paris, France, 1998 (unpublished).
40019. A. P. Serebrov, presented at the International Workshop on Particle Physics with
401 Slow Neutrons Inst. Laue Langevin, Grenoble, France, 2000 (unpublished).
40220. A. P. Serebrov, V. A. Mityukhlyaev, A. A. Zakharov, T. Bowles, et al., JETP Letters **66**
403 (12), 802-808 (1997).

A. Anghel, F. Atchison, B. Blau, B. van den Brandt, et al., Nuclear Instruments and Methods in Physics Research, Section A: Accelerators, Spectrometers, Detectors and Associated Equipment **611** (2-3), 272-275 (2009).

A. Frei, I. Altarev, E. Gutsmiedl, F. J. Hartmann, et al., Verhandlungen der Deutschen Physikalischen Gesellschaft **43** (3), 1 pages (2008).

Y. Masuda,"*Ultra cold neutron production with medium energy proton accelerator*",World Scientific Publishing Co. Pte. Ltd, Singapore (Singapore), Report No. 981-238-125-2, 2002.

E. Korobkina, B. Wehring, A. Hawari, A. Young, et al., Nuclear Instruments and Methods in Physics Research Section A: Accelerators, Spectrometers, Detectors and Associated Equipment **579** (1), 530-533 (2007).

C. L. Morris, J. M. Anaya, T. J. Bowles, B. W. Filippone, et al., Phys. Rev. Lett.**89** (27), 272501 (2002).

C. Y. Liu, A. R. Young and S. K. Lamoreaux, Physical Review B **62** (6), R3581-R3583 (2000).

A. Saunders, J. M. Anaya, T. J. Bowles, B. W. Filippone, et al., Physics Letters B **593**, 55-60 (2004).

F. Atchison, B. Blau, K. Bodek, B. van den Brandt, et al., Nuclear Instruments and Methods in Physics Research, Section A: Accelerators, Spectrometers, Detectors and Associated Equipment **611**, 252-255 (2009).

C. M. Lavelle, C. Y. Liu, W. Fox, G. Manus, et al., Physical Review C (Nuclear Physics) **82** (1), 015502 (015514 pp.) (2010).

R. E. Hill, (2004).

R. C. P. C.-. Monte Carlo N-Particle Transport Code System Including MCNP5 1.51 and MCNPX 2.6.0 and Data Libraries, (2008), pp., 2008.

X-5-Monte-Carlo-Team,"*MCNP-a Genral Monte Carlo N-Particle Transport Code, Version 5*",Los Alamos National Laboratory, Report No. LA-UR-03-198, 2003.

D. B. Pelowitz-editor,"*MCNPX User's Manual, Version 2.6.0*",Los Alamos National Laboratory, Report No., 2008.

Y. Xu, North Carolina State University, 2006.

F. Atchison, B. Blau, K. Bodek, B. Van Den Brandt, et al., PHYS. REV. LETT.**99** (26), 262502 (2007).

C. L. Morris, T. J. Bowles, J. Gonzales, R. Hill, et al., Journal Name: Nuclear Instruments and Methods in Physics Research. Section A, Accelerators, Spectrometers, Detectors and Associated Equipment **599**, 248-250 (2009).

C. Y. Liu, S. K. Lamoreaux, A. Saunders, D. Smith, et al., Nuclear Instruments & Methods in Physics Research Section A **508** (3), 257-267 (2003).

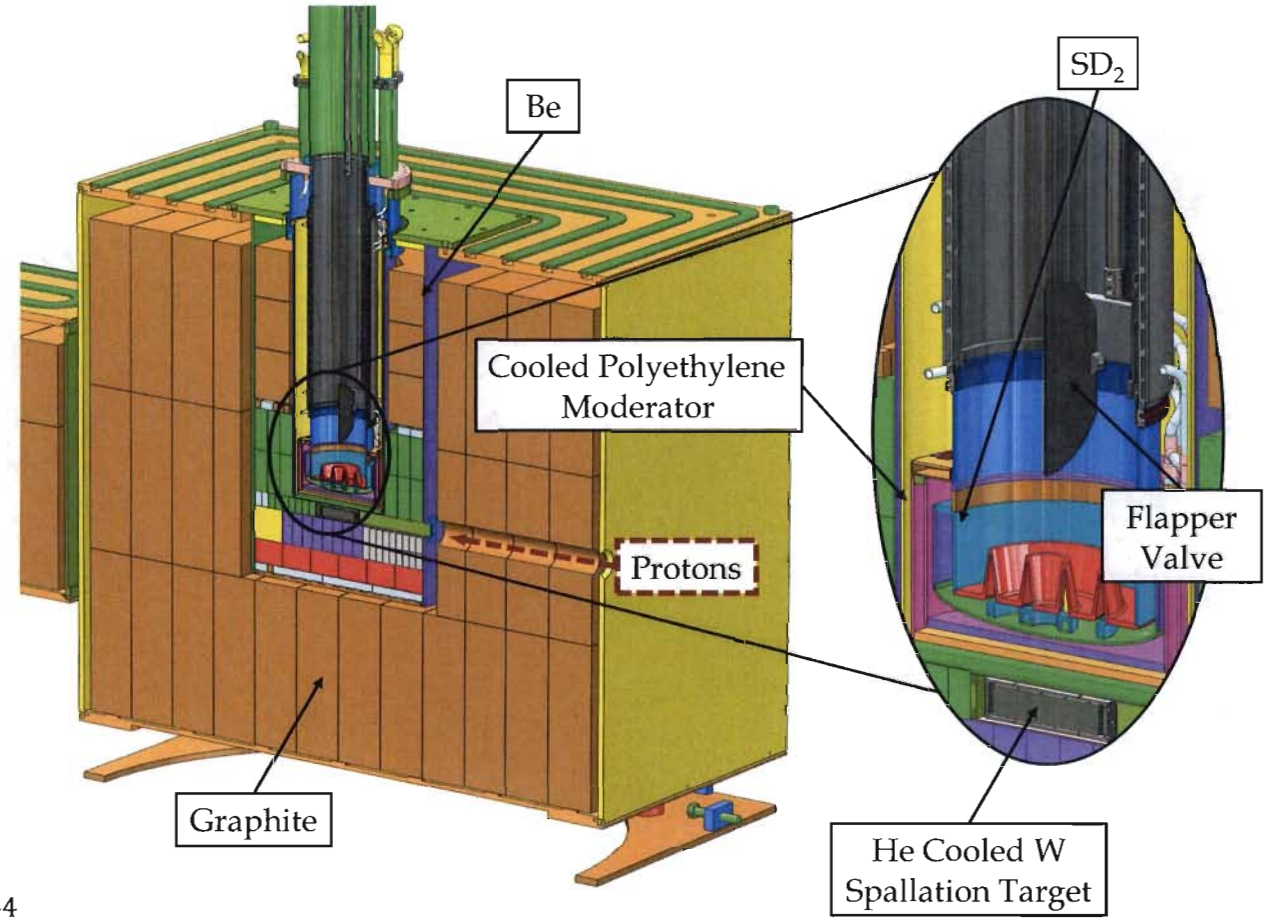

Figure 1) Cutaway view of the source.

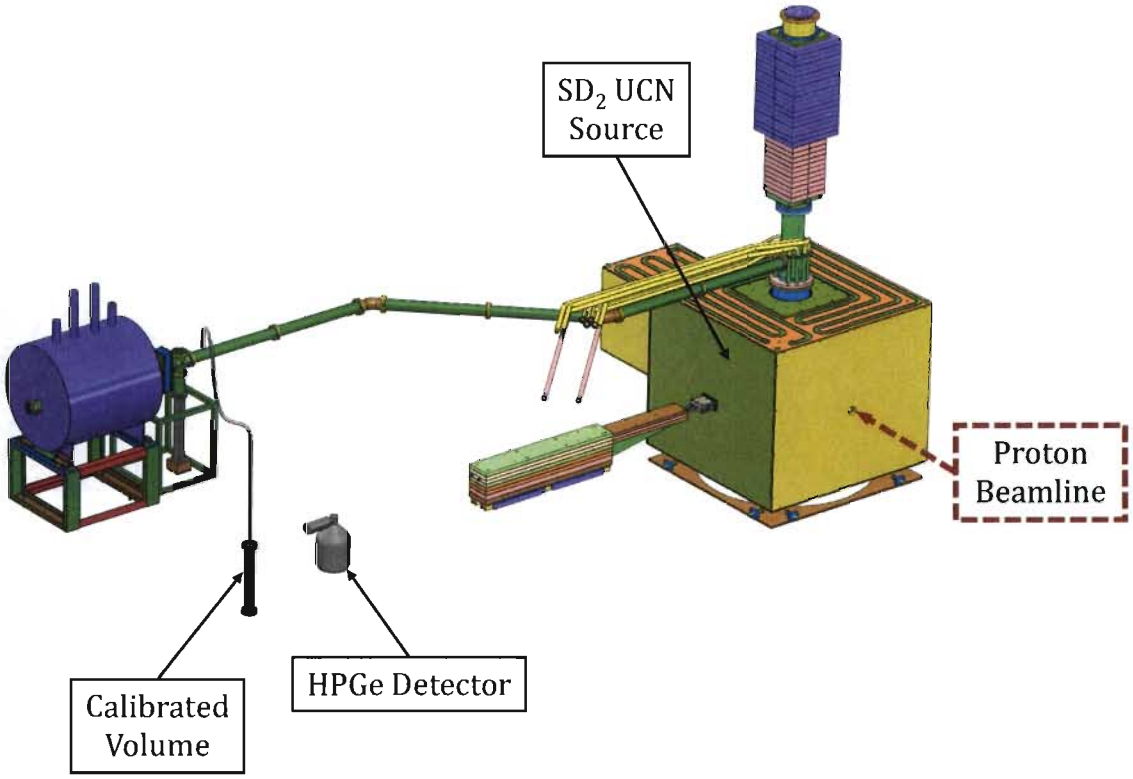

Figure 2) Schematic layout of the argon activation experiment.

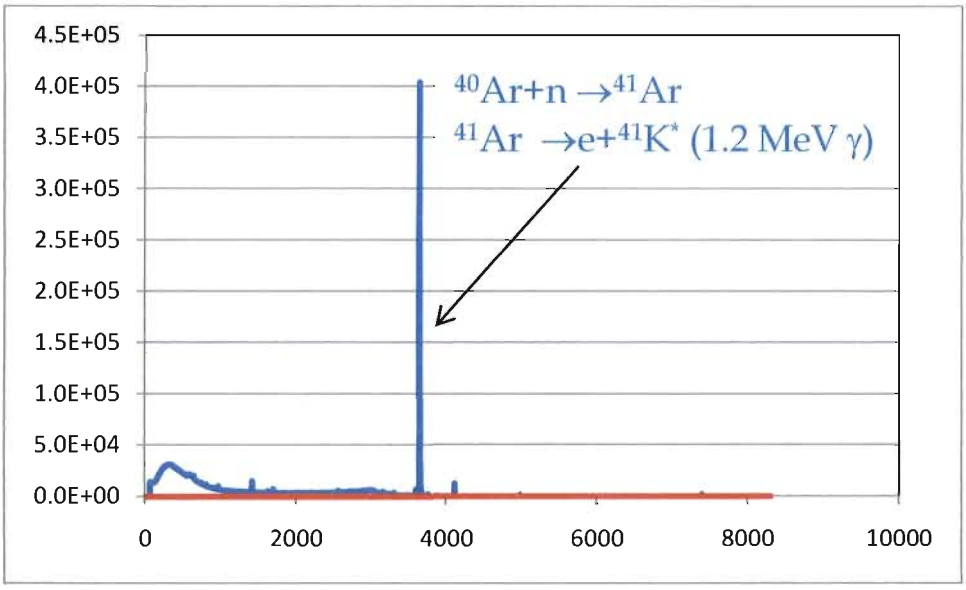

Figure 3) Spectrum of gamma rays from the irradiated argon (blue) and the background (red).

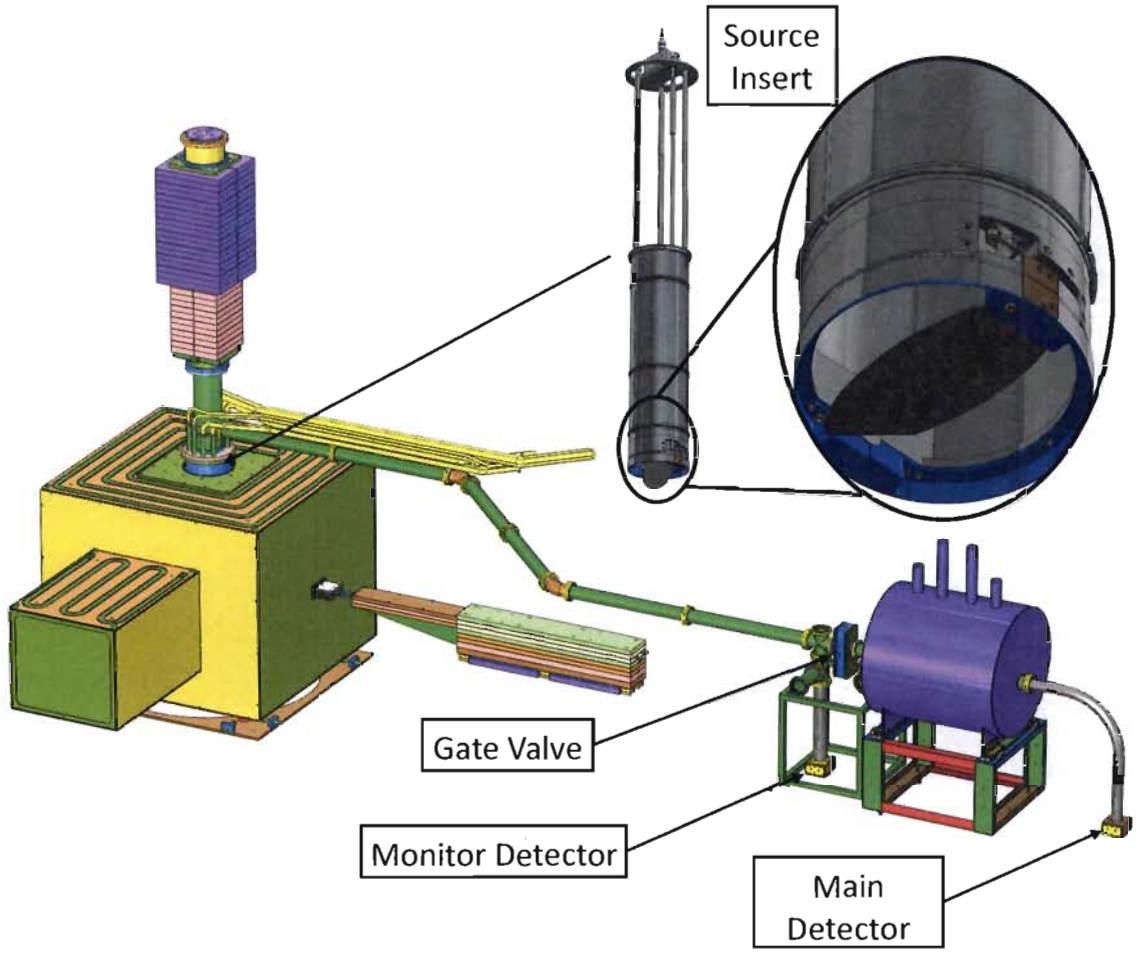

Figure 4) Experimental configuration used to measure the external source performance. The top insert shows the details of the flapper valve and the lower insert (need to add) shows the details of the detector system that was exterior to the shielding package.

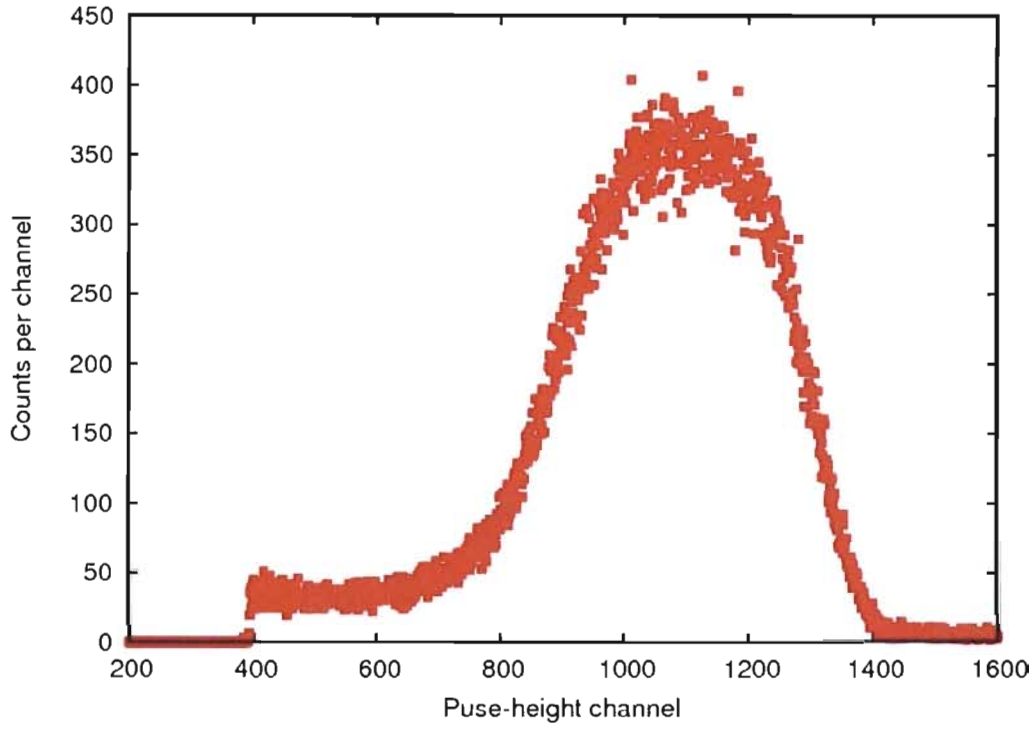

Figure 5) Pulse-height spectrum from the 3He detector.

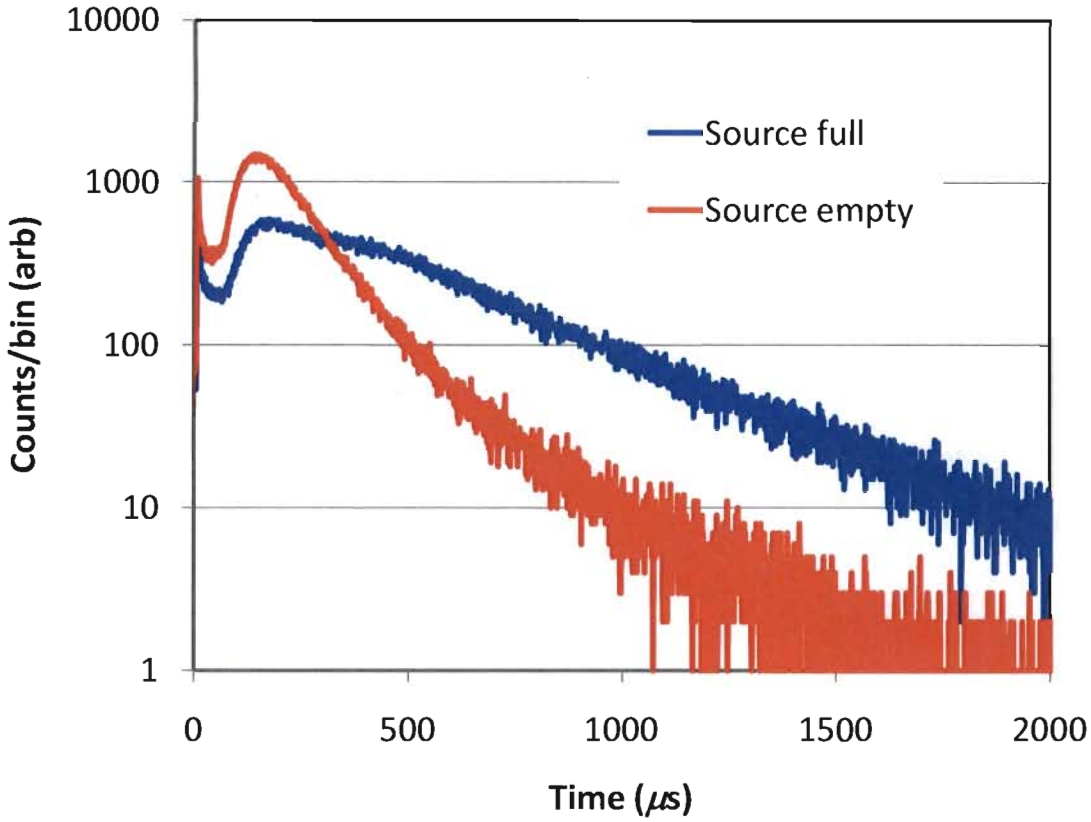

463

464Figure 6) Time-of-flight spectrum with the source empty (red) and full (blue). The polyethylene
465temperatures were 220K and 60K respectively.

466

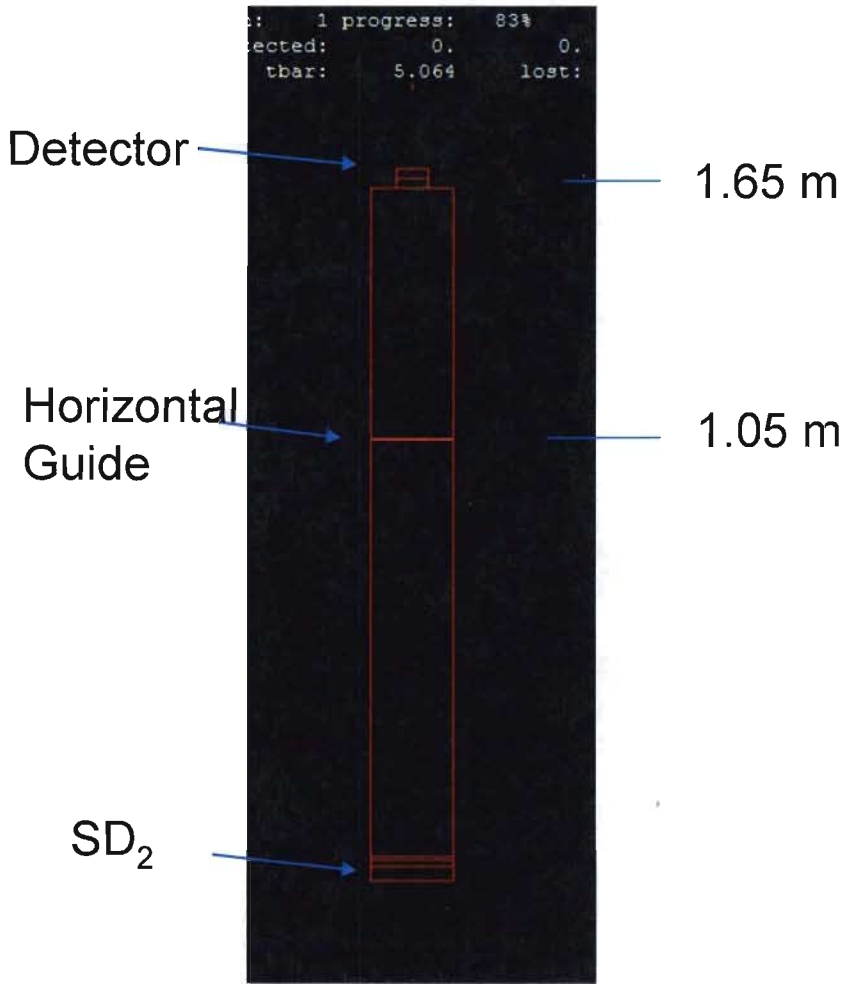

Figure 7) Geometry used in the simulations.

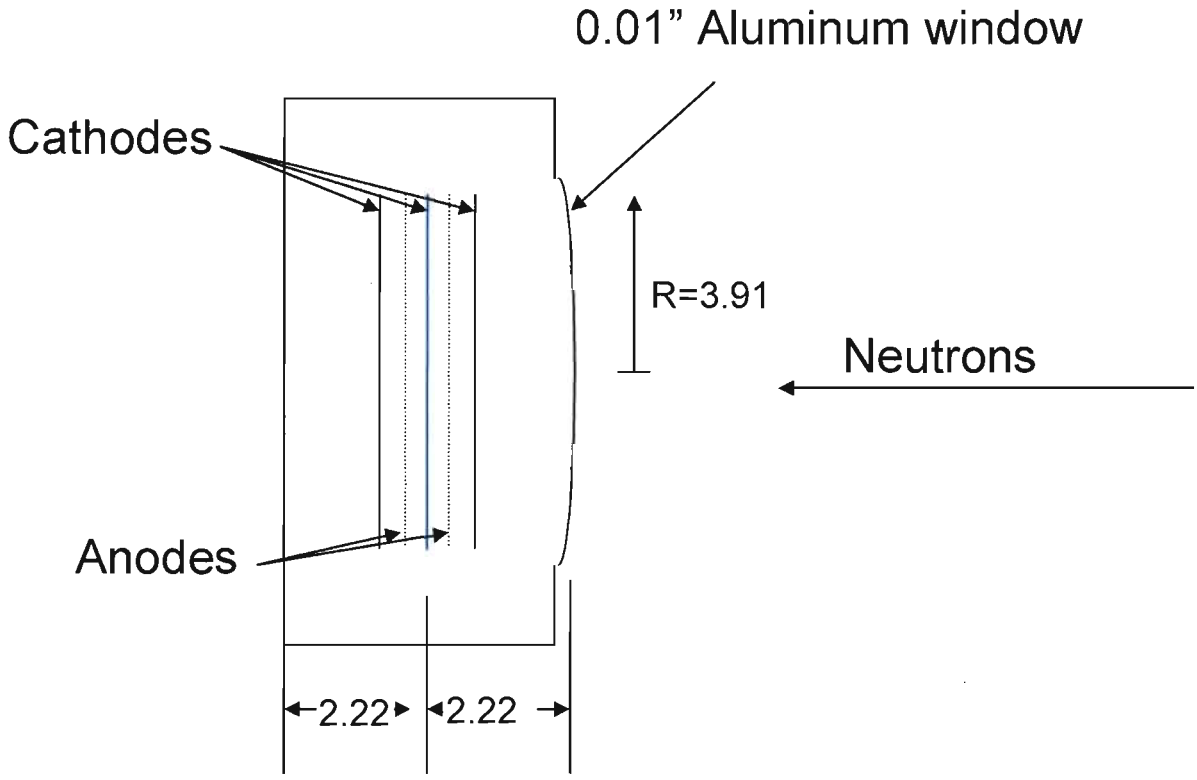

Figure 8) Schematic view of the detector.

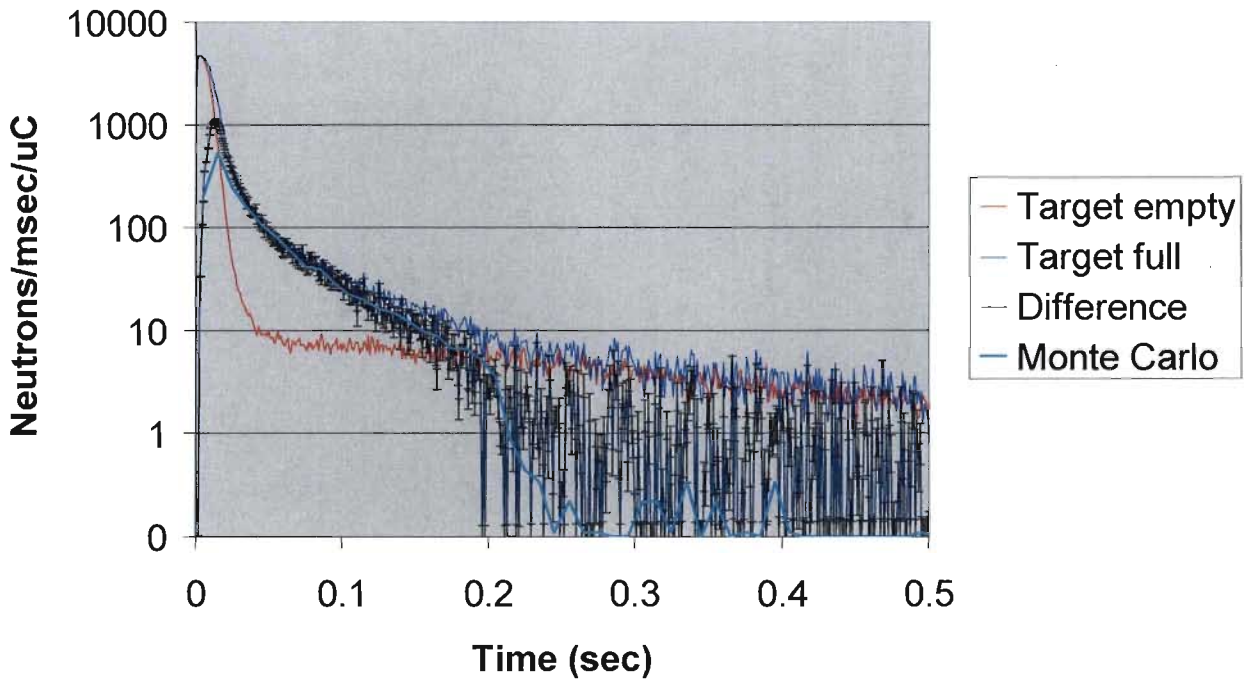

Figure 9) Monte Carlo compared to the data.

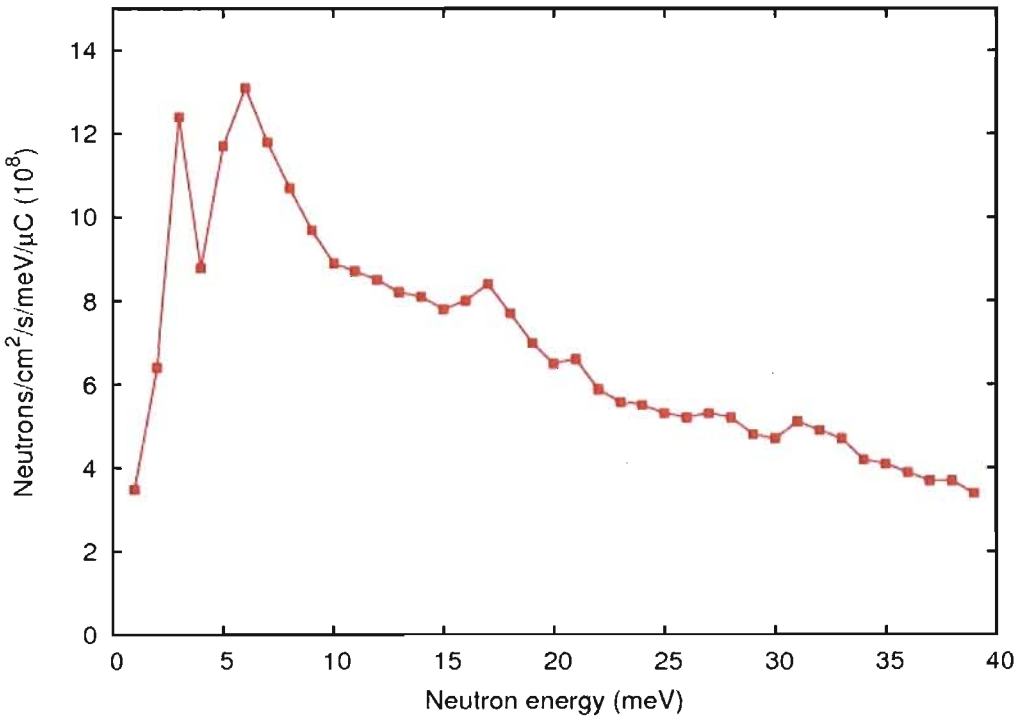

Figure 10) MCNP simulated cold neutron flux for the LANL ultra cold neutron source.

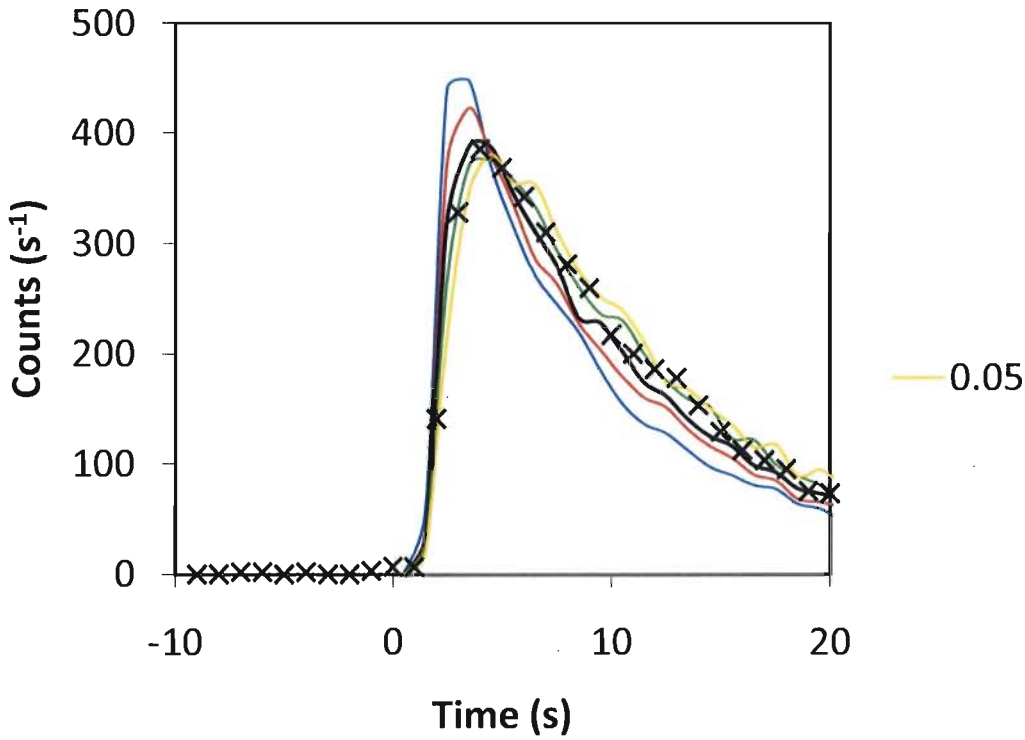

Figure 11) UCN lifetime measurements with the flapper valve open. The curves show the Monte Carlo predictions for different values of the guide non-speculatity.

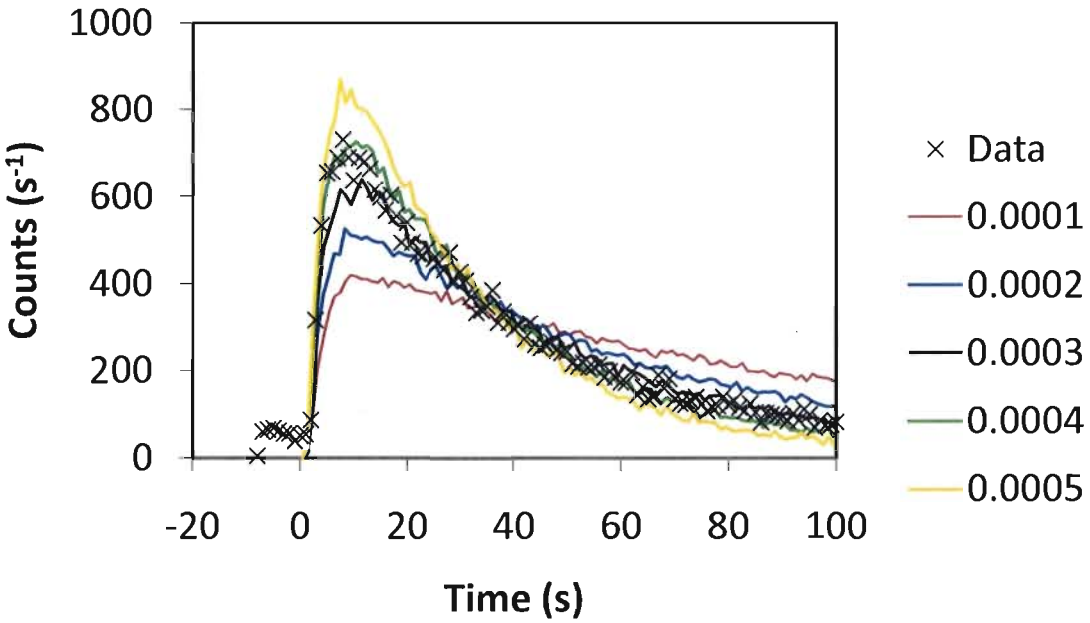

Figure 12) Flapper closed lifetime measurement. The solid lines show Monte Carlo predictions for different loss per bounce values.

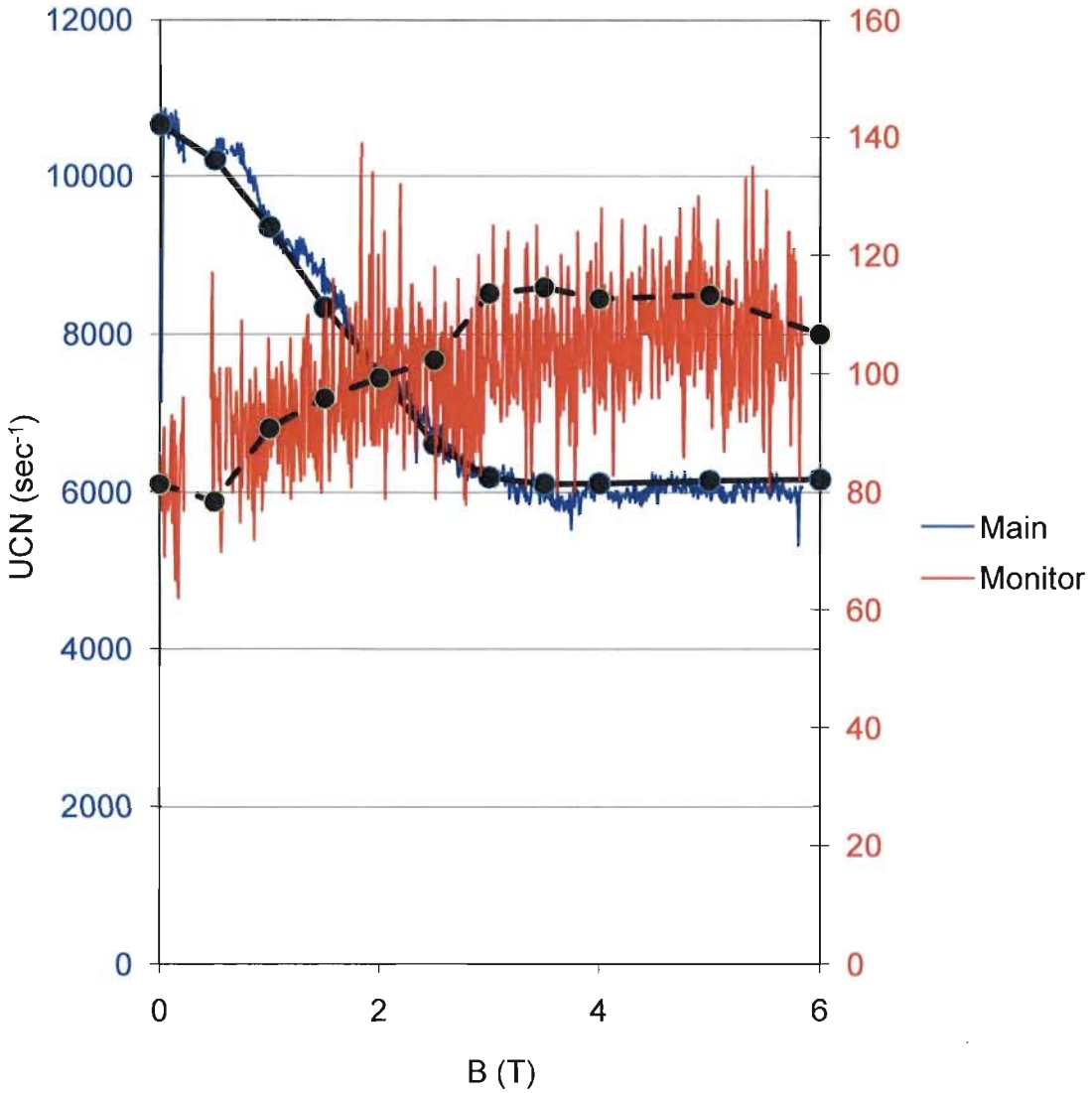

Figure 13) Main (blue) and Monitor (red) detector counting rates as a function of the magnetic field in the pre-polarizer magnet. The black curves show the Monte Carlo predictions.

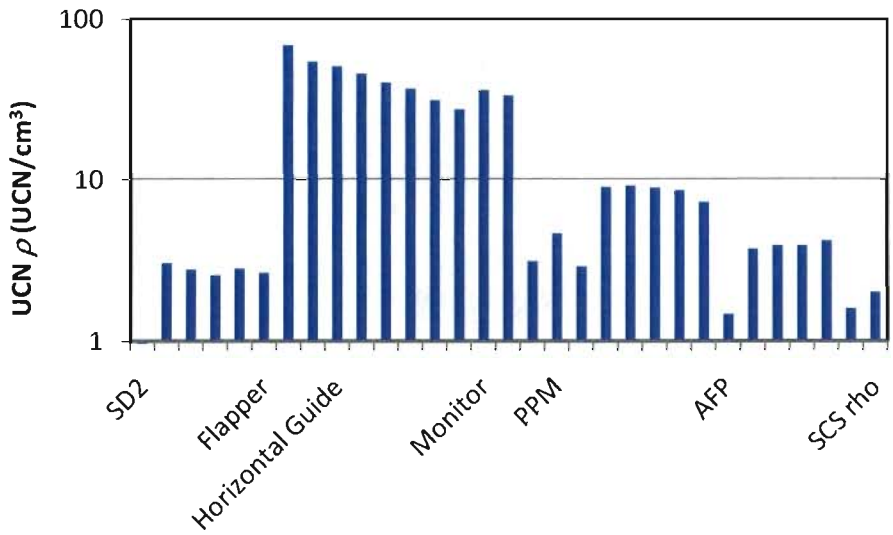

Figure 14) UCN density in the transport elements between the source and the SCS. There are three super conducting magnets in the transport, the PPM with a 6 T field, the Adiabatic Fast Passage spin processor magnets with a short section of 7 T field and a gradient section of 1 T, and the SCS with a 1 T field.